A Software-Based Receiver Sampling Frequency Calibration Technique and its Application in GPS Signal Quality Monitoring

Yanhong Kou, Xingyun Zhou, *Beihang University, China*
Yu Morton, *Miami University*
Dennis M. Akos, *University of Colorado- Boulder*

BIOGRAPHY

Yanhong Kou is an associate professor in the School of Electronic and Information Engineering at Beihang University, China. She received a Ph.D. in Electrical Engineering from Beihang University. Her research interests are in GNSS simulators, high performance receivers, digital signal processing, and wireless communication.

Xingyun Zhou is a master degree candidate in the School of Electronic and Information Engineering at Beihang University, China. He received a B.S. from Dalian University of Technology, China in July 2008. His research interests are in GNSS software receivers.

Dr. Yu (Jade) Morton is a Professor in the Department of Electrical and Computer Engineering at Miami University. She holds a PhD in Electrical Engineering from Penn State. Her current research areas are in software radio techniques, high performance GPS receiver design, radar remote sensing and modeling of the ionosphere, and navigation applications.

Dennis M. Akos completed the Ph.D. degree in Electrical Engineering at Ohio University within the Avionics Engineering Center. He has since served as a faculty member with Luleå Technical University, Sweden, and then as a researcher with the GPS Laboratory at Stanford University. Currently he is a faculty member with the Aerospace Engineering Science Department at the University of Colorado, Boulder.

ABSTRACT

Due to manufacturing and environmental reasons, a GPS receiver's actual and manufacturer specified sampling frequency may differ significantly. Accurate knowledge of the sampling frequency is fundamental for high sensitivity and high accuracy receiver signal processing. Additionally, applications such as pre-correlation signal quality monitoring employing periodic averaging and dithered sampling techniques to enhance the signal-to-noise ratio (SNR) and sampling resolution depend on the accuracy of the sampling frequency. A refined mathematical model of software-correlator based receiver processing in the presence of clock error is established in the paper, and a novel inline method is presented to estimate the accurate sampling frequency. The method is a solely software-based technique requiring no additional hardware other than the GPS receiver RF front end output samples. Neither a priori knowledge of the specific frequency plan of the RF front end circuit nor complex receiver output data fitting are needed. The impact of the sampling frequency error on the performance of receiver signal processing and pre-correlation periodic averaging, and the performance of the frequency calibration method are evaluated using simulated signals as well as live GPS signals collected by GPS data acquisition equipments manufactured by different vendors. Several experimental measurements are presented to support the evaluation including the receiver observables and navigation solutions, as well as the pre-correlation time domain waveforms and eye patterns, Power Spectrum Density (PSD) envelopes, amplitude probability density histograms, correlation function and S-curve bias after periodic averaging. Our simulation results show that the method can calibrate the sampling frequency with an accuracy resolution down to 10^{-9} of the true sampling frequency online, and the pre-correlation SNR can be potentially improved by 39dB using periodic averaging.

INTRODUCTION

A digital GPS receiver extracts measurements from the processing of digitized GPS signals in step with its own local oscillator [1]. Due to manufacturing and environmental effects (such as aging, temperature/power supply fluctuation, platform acceleration, Ionizing radiation, etc.), the oscillator's true output frequency often

deviates from its nominal frequency specified by the manufacture. On the other hand, the oscillator's frequency error characteristics will impose a comprehensive impact on receiver performance [2]. The accuracy and stability of the oscillators in the front-end hardware affect both the IF and ADC sampling frequency and impact the receiver performance through different mechanisms [3]. Oscillator induced digital IF offset and its impact on GPS receiver performance have been summarized in [4]. Although it is well known that both the clock bias and the clock drift can be solved as byproducts of the GPS navigation solution, it makes sense to further investigate the effect of sampling frequency error, especially for software-based receiver implementations, where the local reference signal is actually generated using an assumed sampling frequency instead of the true sampling frequency of the incoming signal. An accurate knowledge of the sampling frequency is essential for high sensitivity and high accuracy receivers. Additionally, applications such as pre-correlation signal quality monitoring employing periodic averaging and dithered sampling techniques to enhance the signal-to-noise ratio (SNR) and sampling resolution also places stringent requirement on the accuracy of the sampling frequency [5].

Several previous methods were developed to calibrate the oscillator frequency without the use of dedicated hardware such as a frequency counter. For example, [3] presented a technique to estimate the sampling frequency by fitting receiver output. This technique, however, requires knowledge of the specific frequency plan of the RF front end circuit. And it is based on the signal acquisition and open loop estimation of initial code and carrier phase velocities obtained through an L1 software GPS receiver. As a result, its calibration accuracy is limited. [6] presented a sampling frequency estimation method for the purpose of clock steering to maintain the receiver time within a certain range from the GPS time and to report the position /measurements on integer seconds. The method interpolates raw code and carrier phase measurements in each tracking channel at the common receiver time to extract reported pseudorange and carrier phase observables. For the clock errors, the digital IF and the sampling frequency are assumed to be derived from the same oscillator.

This paper presents a solely software-based method to estimate the accurate sampling frequency and digital IF of a GPS RF front end using the front end ADC output samples without any additional hardware and a priori knowledge of the RF front end frequency plan. The method derives both IF and sampling frequency errors from closed loop tracking outputs and PVT solutions. It is applicable in the cases with any number of frequency sources used in the RF down-converter and the digital IF signal collecting hardware. The method employs extended averaging in the measurements and solution domain to yield high accuracy calibration results. Moreover, a measurements extraction and clock-steering mechanism different from the method in [6] are proposed, where the raw measurements can be roughly aligned to the integer intervals (any multiples of the raw measurement extraction interval) of GPS time after obtaining the estimation of clock errors, and then the reported position/measurements can be further interpolated onto the exact integer intervals of GPS time.

The paper organization is the following. Section 2 will present the refined signal model in the presence of the sampling frequency error and derive our proposed frequency calibration methodology. Section 3 will provide the experimental measurements and subsequent processing results using the simulated signals and live GPS signals from different sources. The impact of sampling frequency error on the performance of software receiver signal processing as well as periodic averaging, and the frequency calibration accuracy are evaluated by these results.

SIGNAL MODEL AND METHODOLOGY

The performance evaluation of receiver signal processing and pre-correlation signal quality monitoring is based on the refined signal model in the presence of sampling frequency error in a software-correlator based GPS receiver. The proposed frequency calibration approach is also deduced from the signal model in this section.

The GPS L1 C/A signal transmitted by a satellite at GPS system time t can be expressed as

$$s(t) = AD(t)C(t)\cos(2\pi f_L t + \varphi) \tag{1}$$

where A, f_L, φ denote the amplitude, frequency, phase of the transmitted BPSK carrier signal respectively; $D(t)$ is the navigation message signal with the data bit stream D_m:

$$D(t) = \sum_{m=-\infty}^{\infty} D_m \mathrm{rect}\left(\frac{t}{20460T_{C0}} - m\right) \tag{2}$$

And $C(t)$ is the PRN code signal with the code sequence C_i, a period of N=1023 and a chip rate of $f_{C0} = 1/T_{C0} = 1.023MHz$:

$$C(t) = \sum_{m=-\infty}^{\infty}\sum_{j=0}^{19}\sum_{i=0}^{1022} C_i \mathrm{rect}\left(\frac{t}{T_{C0}} - (i + 1023j + 20460m)\right) \tag{3}$$

where $\mathrm{rect}(x) = \begin{cases} 1 & 0 \le x < 1 \\ 0 & \text{other} \end{cases}$.

The signal is propagated through the wireless channel, received by the receiver antenna, amplified, filtered, down-converted and digitized by the receiver front-end into a digital IF signal:

$$s_{IF}(nT_S) = A_{IF} D\left[nT_S(1+\gamma_{Cd}) - \tau\right] \cdot C\left[nT_S(1+\gamma_{Cd}) - \tau\right] \cos\left[2\pi(f_{IF} + f_d)nT_S + \phi\right] \quad (4)$$

where we put the reference point of the signal model at the entrance of the digital correlator in the receiver. τ is the group delay of the propagation channel, f_d is the carrier Doppler shift corresponding to the relative velocity of the satellite and the receiver along the line-of-site (LOS) path, $\gamma_{Cd} = f_{Cd}/f_{C0}$ is the relative code Doppler, f_{Cd} is the code Doppler, ϕ is the carrier phase, and A_{IF} is the amplitude. The relative code Doppler γ_{Cd} can be approximated by the relative carrier Doppler $\gamma_d = f_d/f_L$ if we ignore the code and carrier rate divergence. For the analysis of batched digital signal processing, these parameters are considered constant in one batch of samples, and γ_{Cd} and γ_d can be explicitly formulated using different τ and ϕ values from consecutive batches instead of being embedded in the derivatives of τ and ϕ [7]. $T_S = 1/f_S$ is the true sampling interval with f_S being the true sampling frequency. f_{IF} is the digital IF and is related to the analog IF by this formula:

$$f_{IF} = \left| f_{AIF} - \frac{q}{2} f_S \right| \quad (5)$$

where q is an integer, $f_{AIF} = |f_L - f_{LO}|$ is the analog IF, $f_{LO} = \pm f_{LO1} \pm \cdots \pm f_{LOp}$ is the local reference frequency of the p stage down-conversion in the receiver front-end. For example, $p = 1$ and $f_{LO} = f_L$ refer to direct conversion to zero IF, while $p = 0$ and $f_{LO} = 0$ correspond to direct RF sampling. The "+" and "-" signs are determined by the frequency plan. The sampling process generates periodic replications of the original double-sided spectrum of the analog IF signal. If the baseband spectrum is the translation of the negative frequency part of the original double-sided spectrum (which is also called "aliasing" in the sub-sampling process), there will be an inversion of the frequency and phase error/offset in the received signal. The Doppler frequency (phase change) will be inversed and an error term induced by the sampling frequency error will be added to the total frequency error of the digital IF [4]. The resulting digital IF offset from its nominal value caused by oscillator error is usually treated as user clock drift and resolved in the PVT solution directly. But the analysis later in this section shows that in addition to this digital IF offset, the sampling frequency error will also contribute to the above-solved clock drift in a software-correlator based receiver. While the total clock drift can be easily resolved in the PVT solution, the sampling frequency error has other implications.

The receiver correlates the incoming digital signal with a locally generated reference signal to obtain the dispreading gain for further processing, in the form of either a time-domain MAC correlator or an equivalent frequency-domain multiplier or a passive matched filter. The local reference signal in the software correlator can be expressed as:

$$s_L(n\hat{T}_S) = C\left[n\hat{T}_S(1+\hat{\gamma}_{Cd}) - \hat{\tau}\right] \cdot \cos\left[2\pi(\hat{f}_{IF} + \hat{f}_d)n\hat{T}_S + \hat{\phi}\right] \quad (6)$$

where the symbol $\hat{x}$ denotes the receiver estimated value of the quantity x. The estimation error is $\Delta x = \hat{x} - x$. Not knowing the exact true sampling frequency f_S, the receiver processes the signals in its estimated sampling frequency $\hat{f}_S = 1/\hat{T}_S$ with a relative error

$$\gamma_S = (\hat{f}_S - f_S)/f_S = \Delta f_S / f_S \quad (7)$$

The synchronization (including the coarse acquisition and the refined tracking) of the local signal with the incoming signal is actually an alignment between two discrete sample sequences [8]. The frequency synchronization state will be achieved if the local sample sequence in equation (6) "matches" the incoming sample sequence in equation (4) when a set of estimated parameters ($\hat{f}_s$, $\hat{f}_{IF}$, $\hat{f}_d$, $\hat{\gamma}_{Cd}$) satisfy the following two equations:

For carrier synchronization

$$\frac{\hat{f}_{IF} + \hat{f}_d}{\hat{f}_S} = \frac{f_{IF} + f_d}{f_S} + \delta C_{carr} \quad (8)$$

For code synchronization

$$\frac{f_{C0}(1+\hat{\gamma}_{Cd})}{\hat{f}_S} = \frac{f_{C0}(1+\gamma_{Cd})}{f_S} + \delta C_{code} \quad (9)$$

where δC_{carr} and δC_{code} are the estimation errors with zero mean values. Figure 1 illustrates the concept of the two completely "matched"/synchronized PRN code modulated BPSK waveforms. The local waveform can be a stretched-out or squeezed-in version of the incoming waveform. In terms of digital signal processing the two discrete sample sequences are equivalent to each other although they may be digitized from analog waveforms

with different parameters of carrier frequency, carrier phase, code frequency and code phase. While the IF error will directly result in carrier Doppler measurement error, the sampling frequency error will lead to both carrier and code Doppler measurement error, although the two sample sequences are digitally equivalent.

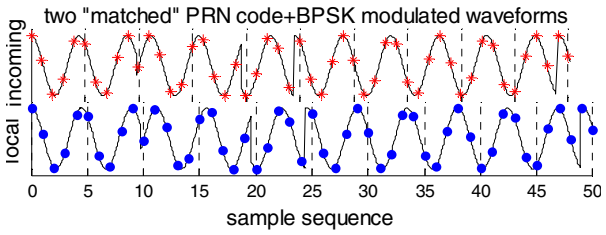

Figure1 Two "matched" PRN code modulated BPSK waveforms

Let's assume that the software receiver has already achieved fine synchronization (phase lock) under an appropriately assumed sampling frequency $\hat{f}_S$ (for example, the nominal sampling frequency) so that the measurements necessary for PVT solutions can be extracted from the code/carrier phase of the synchronized local replica and the demodulated navigation data. Therefore the frequency error between the local code/carrier and the incoming code/carrier will approach zero in a digitally equivalent sense. The carrier measurement $\hat{C}_{carr} = \dfrac{\hat{f}_{IF} + \hat{f}_d}{\hat{f}_S}$ is an unbiased estimation of $C_{carr} = \dfrac{f_{IF} + f_d}{f_S}$, and the code measurement $\hat{C}_{code} = \dfrac{f_{C0}\left(1+\hat{\gamma}_{Cd}\right)}{\hat{f}_S}$ is an unbiased estimation of $C_{code} = \dfrac{f_{C0}\left(1+\gamma_{Cd}\right)}{f_S}$. These two measurements should remain unbiased under different assumed sampling frequency $\hat{f}_S$ and assumed IF $\hat{f}_{IF}$. Calculating 1540*(6)-(7) will lead to another unbiased estimation derived from the former two:

$$\hat{C} = 1540 \times \hat{C}_{code} - \hat{C}_{carr} = C + \delta C \tag{10}$$

$$\hat{C} = \frac{f_L - \hat{f}_{IF} + \left(\hat{\gamma}_{Cd} f_L - \hat{f}_d\right)}{\hat{f}_S} = \frac{f_L - f_{IF}}{f_S} + \delta C \tag{11}$$

where,

$$\begin{aligned} C &= 1540 * C_{code} - C_{carr} \\ &= \frac{f_L - f_{IF} + \left(\hat{\gamma}_{Cd} f_L - f_d\right)}{f_S} \approx \frac{f_L - f_{IF}}{f_S} \end{aligned} \tag{12}$$

$$\delta C = 1540 \times \delta C_{code} - \delta C_{carr} \tag{13}$$

So the relationship of f_{IF} with f_S can actually be measured by $\hat{C}$. Note that there will be a code-carrier Doppler divergence/discrepancy $\left(\hat{\gamma}_{Cd} f_L - \hat{f}_d\right)$ in the receiver measurements caused by Δf_S and/or Δf_{IF}.

The goal is to obtain estimations of three unknown parameters: f_d, f_{IF} and f_S. If the front end circuit frequency plan is known, and the IF error Δf_{IF} and the sampling frequency error Δf_S are coherently derived from the same oscillator, the relationship of Δf_{IF} and Δf_S can be easily given by:

$$\Delta f_{IF} = \gamma_S(\pm f_{LO1} \pm \cdots \pm f_{LOp} \pm \frac{l}{2} f_S) = r\gamma_S f_S = r\Delta f_S \tag{14}$$

where ***r*** is a parameter determined from the frontend circuit's specific frequency plan. Equation (8), (9) and (14) can be jointly solved to determine the three unknowns.

If the frequency plan is unknown, or occasionally the IF error and the sampling frequency error are derived from different frequency sources, we have to find more measurement information than those obtained only from the synchronization process.

As long as the fine synchronization of the code phase and the carrier phase is established in the receiver, the successive bit synchronization, frame synchronization, navigation message decoding, measurements extraction, and PVT calculation can be carried out normally in spite of the frequency offset. After obtaining the receiver position, the receiver clock drift can be resolved based on Equation (8) using the carrier Doppler measurements from more than 4 SV channels:

$$\begin{aligned} \hat{f}_d^j &= \frac{\hat{f}_S}{f_S}\left(f_{IF} + f_d^j\right) - \hat{f}_{IF} + \hat{f}_S \delta C_{carr}^j \\ &= f_d^j - \hat{f}_{IF} + \frac{\hat{f}_S}{f_S} f_{IF} + \gamma_S f_d^j + \hat{f}_S \delta C_{carr}^j \end{aligned} \tag{15}$$

where ***j*** denotes the j^{th} SV tracked. The receiver velocity is embedded in f_d^j and solved either by an LMS estimation or by a Kalman filter, and the clock drift which is common to all the SV channels can be solved as a byproduct:

$$\hat{f}_u = -\hat{f}_{IF} + \frac{\hat{f}_S}{f_S} f_{IF} = -\Delta f_{IF} + \gamma_S f_{IF} \quad (16)$$

As can be seen in this equation, the clock drift solution contains not only the IF error but also an error term caused by the sampling frequency error, and the latter term cannot be neglected.

The clock drift solution can be used to compute the Doppler frequency:

$$f_{d-cali} = \hat{f}_d - \hat{f}_u \quad (17)$$

Substituting (17) into equation (8) and (9), we can solve for the IF and sampling frequencies:

$$f_{IF-cali} = \frac{f_L + f_{d-cali}}{(1+\hat{\gamma}_{Cd}) f_L} \left(\hat{f}_{IF} + \hat{f}_d\right) - f_{d-cali} \quad (18)$$

$$f_{S-cali} = \hat{f}_S \frac{f_{IF-cali} + f_{d-cali}}{\hat{f}_{IF} + \hat{f}_d} \quad (19)$$

Alternatively, we can combine equation (11) and (16) to solve for the calibrated sampling frequency and IF:

$$f_{IF-cali} = \frac{\left(\hat{f}_{IF} + \hat{f}_u\right) f_L}{f_L + \hat{f}_u + \left(\hat{\gamma}_{Cd} f_L - \hat{f}_d\right)} \quad (20)$$

$$f_{S-cali} = \hat{f}_S \frac{f_L}{f_L + \hat{f}_u + \left(\hat{\gamma}_{Cd} f_L - \hat{f}_d\right)} \quad (21)$$

Equation (18) and (19), or (20) and (21) form the foundation of the sampling frequency and IF calibration method proposed in this paper. Both sets of equations can be easily implemented in the receiver software so that the inline calibration of the sampling frequency error can be achieved once the navigation solution is obtained. Thus, the code Doppler and carrier Doppler measurements error due to the sampling frequency error and/or the IF error can also be conveniently corrected online. In the remaining part of the paper, we will present our results based on implementations of equation (20) and (21). Our evaluations of both sets of equations, however, show that they generate similar calibration accuracy of the frequencies.

Moreover, with the continuous and accurate knowledge of the clock bias and the clock drift, the measurements latching and reporting time and such the receiver time of navigation solutions can be steered towards the integer seconds of GPS time. So the clock-steered measurements and navigation solutions can be provided by the receiver. In this paper, we recommend the measurement interrupt mechanism as generally applied in hardware receivers. The measurements of all SV channels are extracted simultaneously at each measurement interrupt. Using the estimation of the difference between the desired integer interval (such as 1ms, 20ms, 1s, etc.) of GPS time and the receiver time of each navigation solution after correcting the clock bias, as well as the solved clock drift, we can adjust the sample number of the measurement interrupt after each navigation solution to the desired value. Consequently, the raw measurements are latched at the samples nearest to the integer intervals of true GPS time, and the impact of sampling frequency error is eliminated in such raw measurements. Since the differences between the measurements latching time and the integer intervals of GPS time are known and are within one sampling interval, the raw measurements and position solutions can be interpolated onto the expected integer intervals of GPS time. The accuracy of the clock-steered results is determined by the accuracy of the navigation solutions.

We recommend choosing one SV with high elevation or high carrier-to-noise-ratio (thus small carrier Doppler and small measurement error), such that the code Doppler $\hat{\gamma}_{Cd} f_{C0}$ and carrier Doppler $\hat{f}_d$ measurements needed in equation (20) and (21) can be averaged over a period from the interval of one position solution to a few seconds, while the clock drift measurements $\hat{f}_u$ can be averaged over an even longer period. The calibrated IF and sampling frequency in equation (20) and (21) can also be averaged to reduce errors. The averaging windows mainly depend on the change rate and the desired update rate of the averaged quantity.

If the uncalibrated sampling frequency offset is beyond a certain value, the receiver will not be able to track some SV channels even after successful acquisitions. When this happens, the TDOP value in the navigation solution may be too high and the above calibration process needs to be repeated under the newly calibrated IF and sampling frequency to refine the solutions. Another benefit of this iteration operation can be seen in equation (15). In addition to the carrier Doppler measurement error of the PLL ($\hat{f}_S \delta C^j_{carr}$), there is another error term $\gamma_S f^j_d$ which depends on the sampling frequency error and is not common to all the SV channels. It is neglected in the clock drift solution because it is a relatively small term considering that a maximum f^j_d of 10KHz and γ_S of 10ppm will lead to less than 0.1Hz error, and it will be significantly reduced after the first time calibration. The first-run calibrated frequencies are accurate enough for most applications so that no iterative implementation is needed and online correcting of code /carrier Doppler is available. For the applications pursuing even higher calibration accuracy, the carrier Doppler measurement error approaches zero when the averaging period increases, and the $\gamma_S f^j_d$ approaches zero with increasing iteration times. So the final calibration accuracy will only be limited by the residual satellite clock drift, the rate of the ionosphere delay, and other factors that contribute to

rate divergences between the group delay and the phase delay of the propagation channel.

EXPERIMENTAL RESULTS AND DISCUSSIONS

In order to investigate the code and carrier measurement performance in the presence of the sampling frequency error, and to examine the calibration accuracy of the algorithm, a set of digital GPS IF signal is generated using a digital IF GNSS signal simulator [9]. The simulated digital IF of the GPS L1 C/A signal is 1.251MHz with a +1KHz error relative to the nominal frequency of 1.25MHz, and the simulated sampling frequency are 5.00005MHz with a +50Hz error relative to the nominal value of 5MHz. The data are processed by a software receiver using different locally assumed sampling frequency. Figure 2 shows the carrier and code Doppler measurements variation with the local sampling frequency ranging from 4999750Hz to 5000350Hz in 50Hz steps. The left top subplot shows that the carrier Doppler measurement $\hat{f}_d$ vary from 2607.906Hz to 2758.347Hz; the right top subplot shows that the measured $\hat{C}_{carr}$ maintains a value of about 0.250734118; the left middle subplot is the code Doppler measurement $\hat{f}_{Cd} = \hat{\gamma}_{Cd} f_{C0}$ varying from -59.618Hz to 63.141Hz; the right middle is the measured $\hat{C}_{code}$ averaged 0.2045983063; the left bottom subplot is the code-carrier Doppler divergence going from -94419.789Hz to 94478.566Hz; the right bottom subplot is the measured $\hat{C}$ averaged 3148.3065757. Equation (8), (9), (11) are validated by these processing results.

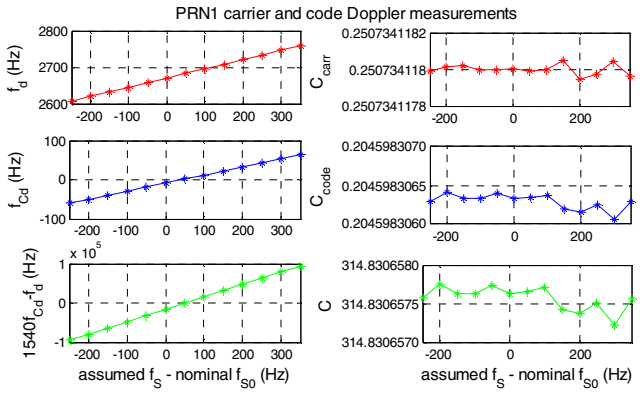

Figure 2 Doppler measurements under different $\hat{f}_S$ using simulated signals

With the simulated signal parameters known, the accuracy of all the measurements in the software receiver can be evaluated. Figure 3 shows the differences between the receiver-measured pseudorange, carrier phase and the corresponding simulator-generated parameters for three different sets of IF and sampling frequencies used in the receiver processing:
Top panel: The IF and sampling frequency assume the nominal values: f_{IF}=1250000Hz and f_S=5000000 Hz.
Middle panel: The IF and sampling frequency take the true values: f_{IF}=1251000Hz, f_S=5000050Hz.
Bottom panel: The IF has the true value f_{IF}=1251000Hz, the sampling frequency f_S=4999950Hz.

The carrier to noise ratio of the simulated IF signal is set to 50dB-Hz, and none of the pseudorange error terms is included in the simulation except the thermal noise. For all three simulation scenarios, the tracking loop parameters of the software receiver have the same values after achieving steady state tracking, and the receiver raw measurements are extracted after achieving the navigation solution with the measurement latching intervals continuously steered. As shown in Figure 3, the clock-steered raw pseudorange and carrier phase measurements show no bias from the simulated values, and present similar noise characteristics in the three cases. As expected, Figure 4 shows that the height error of the position solutions also presents no much difference in the three cases. Extensive test results demonstrate that the sampling frequency error will not impact the accuracy of the code/carrier phase measurements and the consequential PVT solutions when the clock-steering option is turned on, until it is large enough to prevent some SV channels from entering steady state tracking.

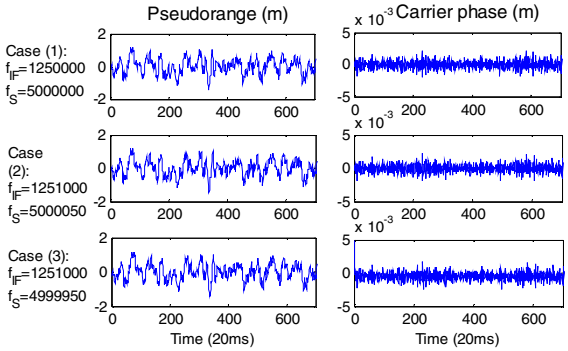

Figure 3 Clock-steered raw pseudorange and carrier phase measurements under different assumed IF and sampling frequency

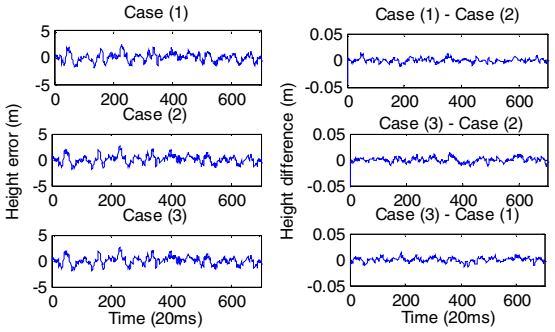

Figure 4 Height errors under different assumed IF and sampling frequency

Using a code/carrier Doppler averaging window of 8s, the first-run frequency calibration accuracy has been evaluated with the initially assumed sampling frequencies ranging from 4999750Hz to 5000350Hz and the initially assumed IF of 1251000Hz. All the seven simulated SVs have been tracked in this frequency error range. The GDOP, HDOP, VDOP and TDOP values are 2.409, 1.108, 1.834 and 1.086 respectively. As shown in Table 1, an online calibration error less than 10^{-9} of the true sampling frequency is guaranteed.

Table 1 Frequency calibration results under different initially assumed sampling frequencies

$\hat{f}_S$ (Hz)	γ_S (ppm)	$f_{IF-cali}$ (Hz)	f_{S-cali} (Hz)	γ_{S-cali} (ppm)
4999750	-59.9994	1251000.188936	5000049.999171	-0.0001658
4999850	-39.9996	1251000.176094	5000050.001896	0.0003792
4999950	-19.9998	1251000.160852	5000050.002867	0.0005734
5000050	0	1251000.145424	5000049.998238	-0.0003524
5000150	19.9998	1251000.131518	5000049.999220	-0.000156
5000250	39.9996	1251000.117598	5000050.003140	0.000628
5000350	59.9994	1251000.101926	5000049.999419	-0.0001162

As a further test using live GPS satellite signals, Figure 5 and Figure 6 give the processing results of the data set "GPS_and_GIOVE_A-NN-fs16_3676-if4_1304.bin" provided by [10]. The local sampling frequency changes in turn from 16367550Hz to 16367556.25Hz with a step of 0.25Hz in Figure 5. The IF and sampling frequency published in [10] are 4130400MHz and 16367600MHz, while the calibrated IF and sampling frequency are 4134846.7Hz and 16367553.679Hz respectively in a 8s window. There is a -46.321Hz deviation of the true sampling frequency from the nominal value, which corresponds to the zero passage point in the left bottom subplot, with a zero code-carrier Doppler discrepancy under the calibrated IF. The top plot in Figure 6 shows the differences between the clock-steered raw measurement latching time and integer multiples of 20ms of GPS time. It can be seen that all the differences are within one sampling interval. The bottom plot shows the corresponding navigation solution results with an updating rate of 50Hz. Another data set in [10] named "GPSdata-DiscreteComponents-fs38_192-if9_55.bin" has also been processed. The published (IF, sampling frequency) are (9548000Hz, 38192000Hz), and the calibrated results are (9547983.8Hz, 38192000.401Hz) for a 8s window.

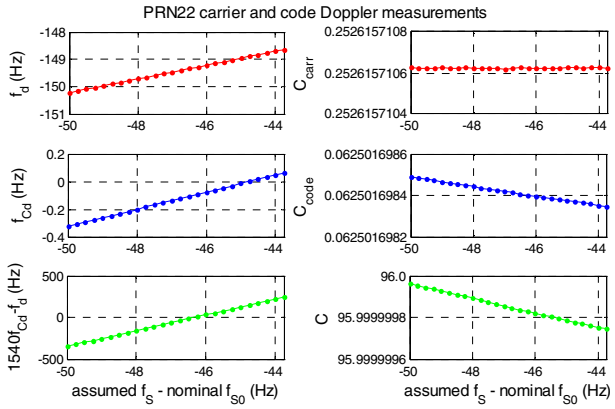

Figure 5 Doppler measurements under different $\hat{f}_S$ using live GPS signals

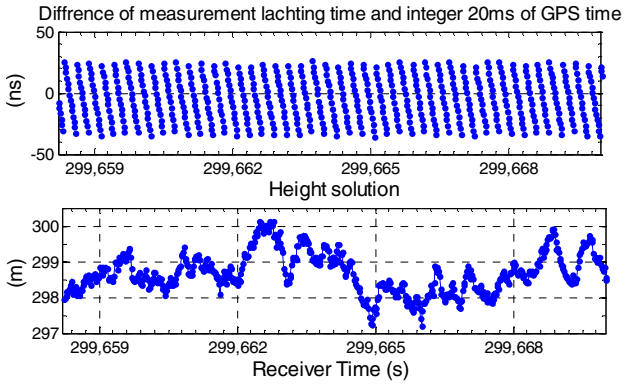

Figure6 Differences between raw measurement latching time and integer intervals of GPS time, as well as height solution using live GPS signals

Data collected from the same Motorola front end used in [3] has also been processed. The nominal values of the (IF, sampling frequency) are (1364000Hz, 5456000Hz), the calibrated results using the method in this paper are (1261722.53Hz, 5455623.421Hz).

The data set "GPSdata-DiscreteComponents-fs38_192-if9_55.bin" is also processed as a case study for the periodic averaging technique, although a wideband frontend is necessary for high fidelity signal quality monitoring. The data are collected using a conventional active hemispheric antenna. The technique applies a sequence of operations on the collected signals of PRN18 at an elevation of 72 deg. The carrier (plus Doppler) and navigation data are wiped off from the incoming signals after achieving tracking and bit synchronization in the software receiver. Then the baseband code signal is periodically averaged and characterized in the time, frequency, modulation and correlation domain. Figure 7 shows the time domain waveforms with different

averaging window using the calibrated sampling frequency and the code chip rate measurement obtained using this sampling frequency. The receiver estimated C/N_0 is 50dB-Hz for PRN18 signals. The received signals are below the noise floor. Averaging 100 code periods results in a 20dB SNR gain which makes the code chip barely visible as the signal level is raised above the thermal noise floor, and the 39dB SNR gain of 8s averaging window leads to a clear code structure in the last subplot. Figure 8 is the corresponding histogram for signal amplitude distribution, which shows the variance of the Gaussian distribution is reduced as the averaging window size increases.

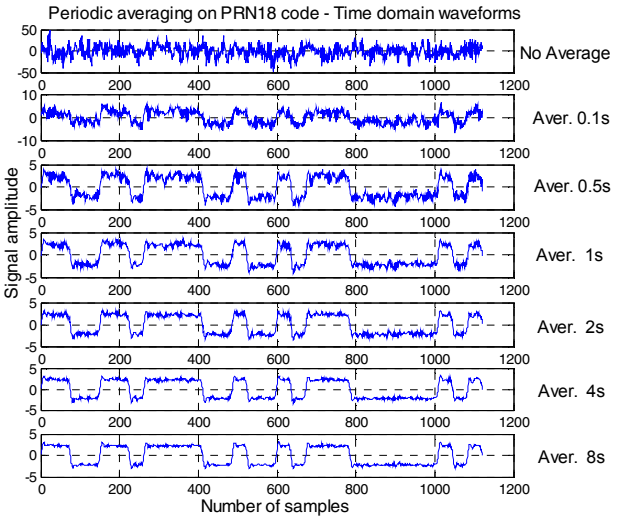

Figure 7 Waveforms with different averaging window

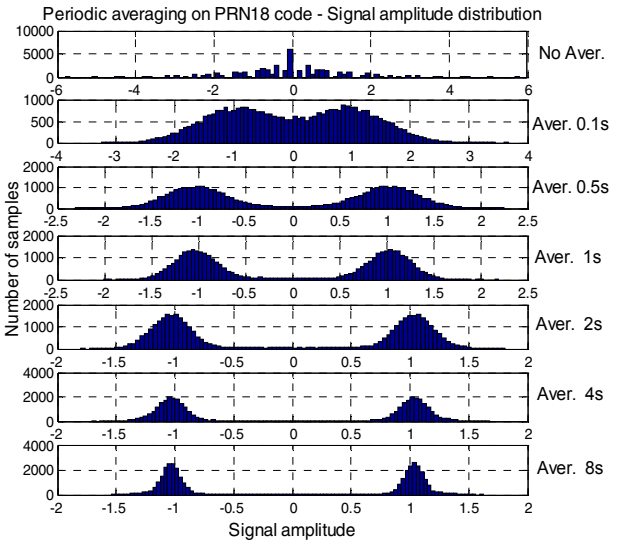

Figure 8 Histograms with different averaging window

Examining the PSDs with different averaging window shown in Figure 9, the top subplot shows only the thermal noise floor and the filtering effect of the frontend, while a 8s averaging raise several side lobes above the noise in the bottom subplot. Figure 10 and Figure 11 depict the zoomed in view of the individual code chip and the eye pattern after averaging over 8000 code periods. The ring phenomenon induced by the limited frontend filter bandwidth is evident. Figure 12, 13 show the CCF of the incoming PRN18 code with the ideal local code and the S-curve bias of the incoming code signal respectively after averaging over 8000 code periods. A non-coherent early minus late power discriminator is used in the S-curve analysis. As a contrast, Figure 14 shows the CCF without averaging, as well as the autocorrelation function (ACF) of an ideal PRN18 code sequence. It can be seen that the SNR gain introduced by averaging processing lead to clear signal observation and characterization in the time, frequency and correlation domain.

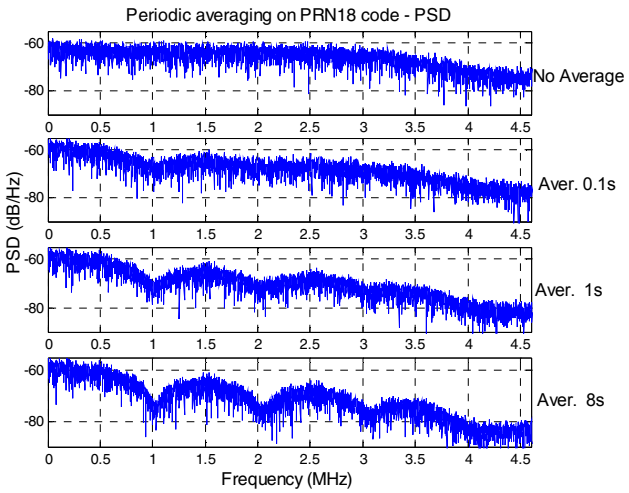

Figure 9 PSDs with different averaging window

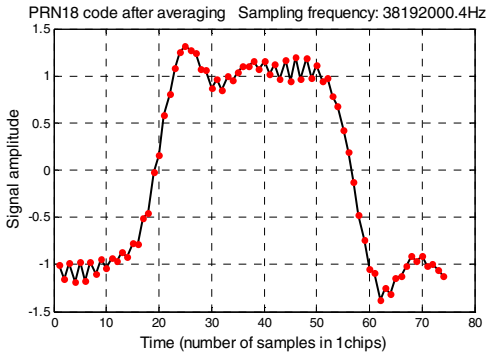

Figure 10 Zoomed in view of one chip after averaging over 8s

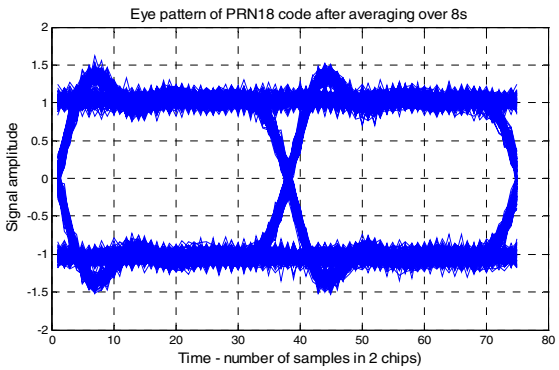

Figure 11 Eye pattern after averaging over 8s

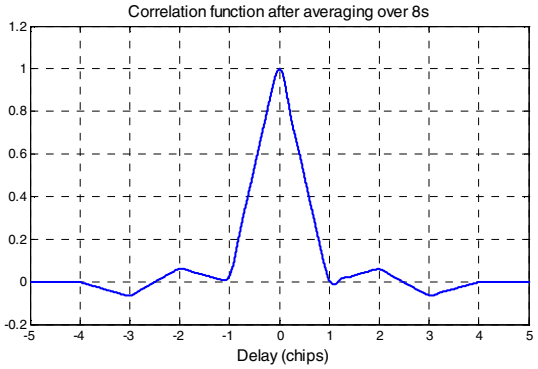

Figure 12 CCF of the incoming code after averaging over 8s with the ideal local code

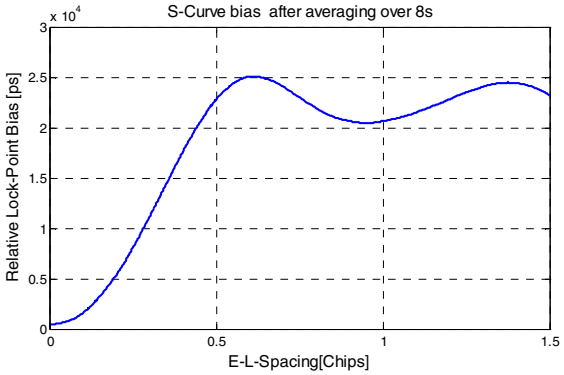

Figure 13 S-curve bias of the incoming PRN18 code signal after averaging over 8s

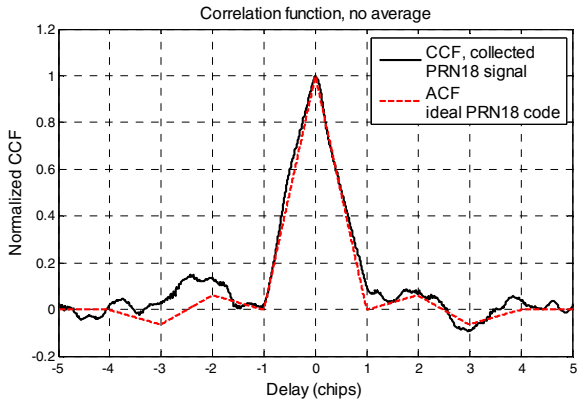

Figure 14 CCF of the incoming code without average, and ACF of the ideal local code

To demonstrate the impact of sampling frequency error on periodic averaging, Figure 15 and 16 show the processing results using a deviated sampling frequency of 38191950Hz. It can be seen that the effectiveness of periodic averaging is degraded by the sampling frequency mismatched the incoming code chip rate. With the averaging window increases, the degradation becomes even severe.

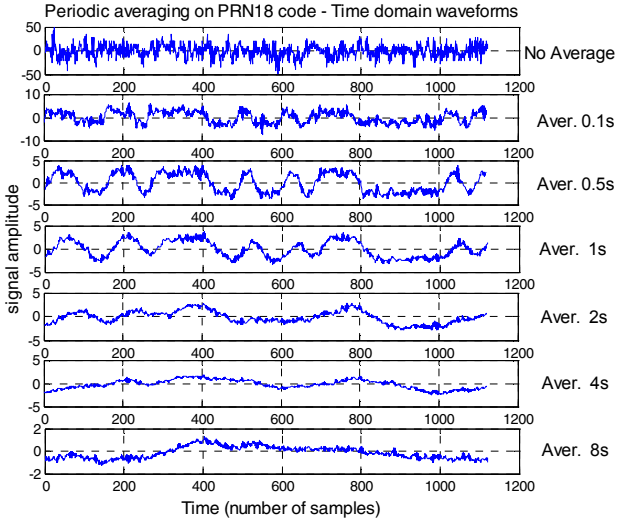

Figure 15 Waveforms with different averaging window under a deviated sampling frequency

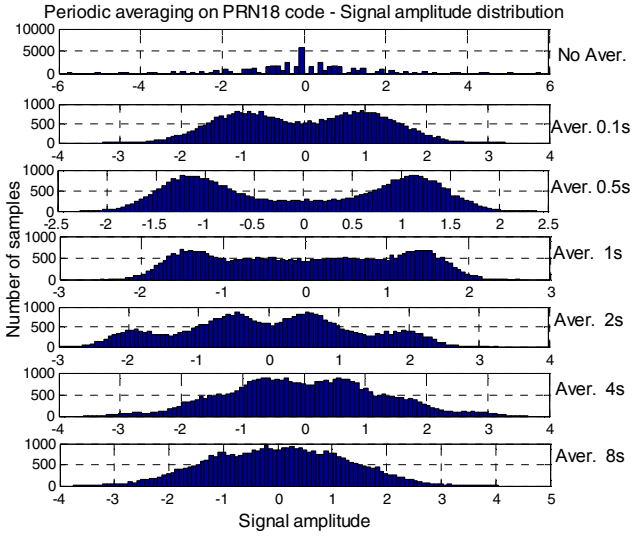

Figure 16 Histograms with different averaging window under a deviated sampling frequency

Figure 17 shows the effect of sampling frequency error on the correlation peak value of the averaged baseband code signal with an ideal local PRN18 code. The frequency step is set to 25Hz (top plot), 2.5Hz (middle plot), and

0.25Hz (bottom plot). The correlation loss is more severe with larger frequency mismatch.

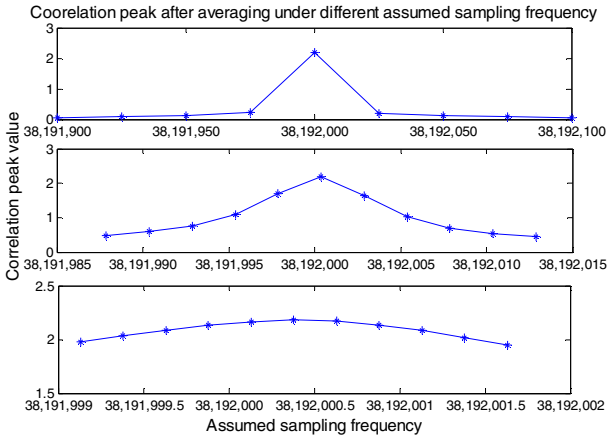

Figure 17 Correlation peak after averaging under different assumed sampling frequency

CONCLUSIONS

This paper has investigated the sampling frequency error impact on the signal processing in a software-correlator based GPS receiver as well as the periodic averaging technique in a pre-correlation GPS signal quality monitor. The refined signal model of receiver processing in the presence of clock error is established as the foundation of the performance analyses. A software-based method is developed to accurately calibrate both the digital IF and the sampling frequency simultaneously. The method requires no additional hardware other than the GPS receiver RF front end output samples. It enables inline calibration of the receiver measurements instead of complicated post-processing. The performance of the technique is evaluated using simulated signals as well as live GPS signals collected by several GPS data acquisition equipments, including clear time domain waveforms/eye patterns, amplitude probability density histograms, Power Spectrum Density (PSD) envelopes, and correlation-related characteristics. The results show that we can calibrate the sampling frequency with an accuracy resolution of 10^{-9} of the true sampling frequency online, and the pre-correlation SNR can be potentially improved by 39dB using periodic averaging.

ACKNOWLEDGMENTS

Yanhong Kou and Xingyun Zhou's work is supported by the Chinese 863 High-tech R&D Program under NRSCC grant 2006AA12Z304 and Chinese NSAF grant 10676002.

REFERENCES

[1] P.W. Ward, "Satellite signal acquisition, tracking, and data demodulation" in E. D. Kaplan and C. J. Hegarty, editor, "Understanding GPS, Principles and Applications (2nd Edition)," Artech House Publishers, p153-242, 2006.

[2] John R. Vig. http://homepage.ntlworld.com/jan.ooijman/quartz_crystal_resonators_and_oscillators_for_frequency_control_and_timing_applications_tutorial.pdf.

[3] L. L. Liou, D. M. Lin, J. B. Tsui, J. Schamus, Y. Morton, "Frequency Characterization of A/D Converter in Software GPS Receivers," Proc. 2005 Joint IEEE Int'l Frequency Control Sym. & Precise Time & Time Interval Sys. & Appl. Meeting, p656-659, Aug. 2005, Vancouver, Canada.

[4] P. M. Corbell. "Design and validation of an accurate GPS signal and receiver truth model for comparing advanced receiver processing techniques," MS thesis of AFIT, OH, March 2000.

[5] M. Pini, D.M. Akos. Exploiting GNSS Signal Structure to Enhance Observability. IEEE Transactions on Aerospace and Electronic Systems, VOL. 43(4), p1553-1566,Oct. 2007.

[6] X. Li, D.M. Akos, Implementation and performance of Clock Steering in a Software GPS L1 Single Frequency Receiver, Navigation: Journal of the Institute of Navigation, Vol.57(1), Spring 2010, to be published.

[7] Y. Kou. "Study on GNSS Software Receiver and Signal Simulator," Beijing University of Aeronautics and Astronautics, China, March 2006.

[8] D. M. Akos, M. Pini, "Effect of Sampling Frequency on GNSS Receiver Performance," Navigation, 2006, VOL 53; No. 2, pages 85-96.

[9] X. Yin, Y. Kou, Z. Zhang. "Design and Implementation of a Flexible Software-based GNSS IF Signal Simulator," Proc. 22nd International Technical Meeting of the Satellite Division ION GNSS 2009, Sept. 22-25, 2009, Savannah, GA.

[10] K. Borre, D. M. Akos, N. Bertelsen, P. Rinder, S. H. Jensen, "A Software-Defined GPS and Galileo Receiver A Single-Frequency Approach," Birkhäuser Boston, Nov. 2006.